REPORT IN THERMOFLUID-DYNAMIC MEASUREMENTS: LASER DOPPLER ANEMOMETRY

TEAM:

Fracchiolla Beniamino;

Giannattasio Marika;

Susca Vito.

A.A. 2021/2022

INDEX

1. Introduction to optical methods **3**

2. Doppler effect **5**

3. System components **9**

4. Laser Doppler Anemometry **11**

5. Physical principle of Laser Doppler Anemometry **16**

6. Discrimination of verse **20**

7. Spatial and temporal resolution **21**

8. Signal form, processing and sampling **22**

9. Accuracy of the LDA system **25**

10. Considerations on tracer particles **27**

11. Use of the instrument **30**

12. Advantages, disadvantages and applications **36**

13. Bibliography **41**

1. INTRODUCTION TO OPTICAL METHODS

A direct velocity measurement of an object requires the estimation of the time it takes to travel a certain known distance. The measured velocity is therefore an average value in space and time given by the:

$$\boldsymbol{v = \frac{\Delta s}{\Delta t}}$$

In optical techniques, the speed signal originates from scattering (or diffusion) centers, typically tracer particles, whose size and density is chosen specifically to prevent sliding with the flow on which you want to perform speed measurements. In fact, only in the absence of sliding is a direct measurement of the local flow velocity performed. The principle of direct speed measurement with optical techniques is illustrated schematically in Figure 1 where the distance S _x is fixed in space by optical methods. In Figure 1 the transmission optics are designed in such a way as to illuminate as clearly as possible the finished width "measuring volume"ΔS_x (the light source may also be inconsistent). A tracer particle will then be illuminated as the measuring volume passes through, producing an extended pulse on the receiver. The width of the pulse Δt is inversely proportional to v_x or the long x component of the particle velocity. This simple principle can be found in a wide variety of measuring instruments, moreover, multiple variations can be achieved by introducing sub-structures to the lighting compartment or the detection compartment. In Figures 1b and 1c a space grid is introduced on the transmitter and receiver sides respectively. Any type of grid can be used, for example a multi-line grid or with only two lines; the latter determines a measurement of the speed by detecting the time of flight as shown in Figure 1d and 1e. The grid is chosen according to practical needs; for example, using a two-line grid would be disadvantageous in the case of very turbulent flow because the trajectory of the particles could be such as to generate the crossing of only one of the two grid lines, which would in fact mean not being able to measure flight time while instead a full lattice solves the speed over the entire measuring volume. In fact, by using lines evenly spaced between them, the velocity perpendicular to these lines is directly proportional to the frequency f of the signal pulses or, indicating with Δx the spacing between the lines and with T the period between two pulses you will have that:

$$\mathrm{v}_x = \frac{\Delta x}{T} = f \Delta x$$

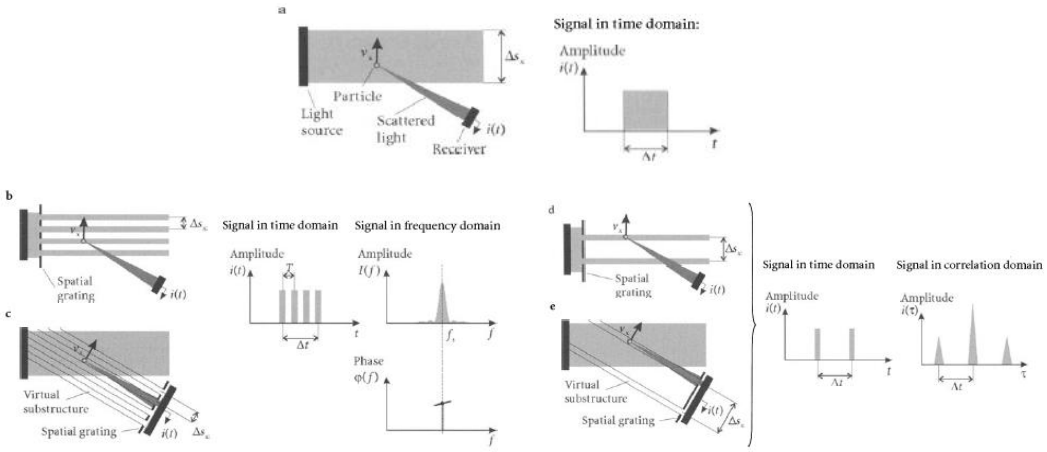

Figure 1 - Flow measurement techniques with optical methods from [1]

In fact, it is not possible to obtain a sufficiently precise and defined measuring volume with a non-coherent light source, and this is one of the reasons why a coherent light source, namely a monochrome laser, is used instead. This consideration leads us directly to the optical configuration known as Laser Doppler. In fact, the Laser Doppler technique could be defined as an optical method that uses a monochromatic laser light source. Monochrome is essential because it ensures the formation of plane wavefronts in phase coherence thanks to which the interference between two rays in the measuring volume or that between two waves scattered on the surface of the photoreceiver, will create a fringed pattern similar to a full reticule in the measuring volume. The velocity information of the particles and therefore of the flow is contained in the electromagnetic field of the same thanks to a physical phenomenon known as the Doppler effect. Therefore, before illustrating the technique, it is appropriate to deepen this effect.

2. DOPPLER EFFECT

Consider a stationary observer and a source of waves also stationary (having wavelength λ and propagation velocity in the middle c), the number of wavefronts intercepted by the observer stationary in the unit of time (frequency) will be simply:

$$f_s = \frac{c}{\lambda} \qquad \left[\frac{m/s}{m} = \frac{1}{s} = Hz = \frac{sample}{s}\right]$$

Now we consider an observer in motion at general speed V towards a stationary source, the latter will intercept a number of wavefronts equal to:

$$f_P = f_s + \frac{V\cos\theta}{\lambda} = \frac{c}{\lambda} + \frac{V\cos\theta}{\lambda}$$

There will then be an apparent increase in the frequency of the radiation perceived by the observer compared to the stationary case given precisely by the second term where V cos θ represents the velocity component in the direction of the source. In fact, with the observer moving towards the source, the wave fronts will have less "space" to travel to reach it.

Figure 2.1a,b - Doppler effect. a Wave frequency from [5], b generic Velocity and component in source direction from [2]

The Doppler effect can therefore be interpreted as an apparent change in the frequency of a wave perceived by an observer who is in motion with respect to the source and vice versa.

Example: when an ambulance approaches, the siren is heard with a sharper tone because the acoustic waves are perceived by the auditory apparatus with a higher frequency. Conversely, when it goes away you hear the sound of the siren with a lower tone as the frequency of the waves increases.

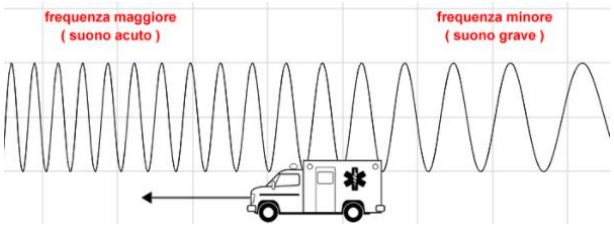

Figure 2.2 - Practical example of the Doppler effect from [5]

The Doppler effect can also be explained by mathematical models. In fact, the propagation of linear waves (acoustic, electromagnetic, etc.) in spacetime is described by the equation of the wave, differential equation of the second order to partial derivatives:

$$\frac{\partial^2 \phi}{\partial t^2} - c^2 \frac{\partial^2 \phi}{\partial x^2} = 0$$

The coefficient c^2 is the square of the propagation velocity of the wave in the medium that is supposed to be constant. It can be demonstrated by substitution that the general integral of this equation is of the:

$$\phi(x,t) = G(x+ct) + F(x-ct)$$

Please note:

- The partial differential equation is of the second order and therefore requires two boundary conditions: one on the temporal variable and one on the spatial variable;
- Due to the dependence on x+ct and x-ct, the functions G and F will describe wave fronts moving left and right of the x-axis with the passage of time;
- The information of these functions is plotted in space-time according to a slope curve $|1/c|$.

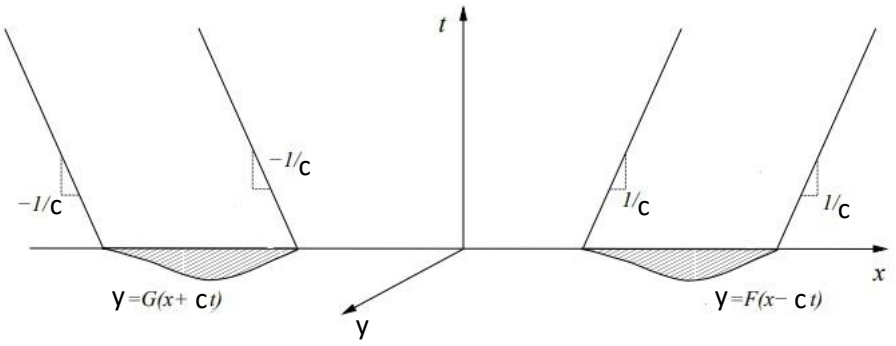

Figura 2.3 – *Rappresentazione delle curve caratteristiche da [4]*

The shape of functions F and G is uniquely defined by the boundary conditions of the problem. In fact, given the following conditions:

$$\begin{cases} \phi(x,0) = f(x) \\ \dfrac{\partial \phi(x,0)}{\partial t} = g(x) \end{cases}$$

The latter will define constraints on the form of the functions F and G:

$$f(x) = F(x) + G(x)$$

$$g(x) = F'(x) + G'(x)$$

It is supposed to place at the time t_0 a transmitter in place x_0 and a receiver in position l, and that the transmitter and receiver move with speed respectively v_1 positive and v_2 negative. The two will meet at some time t identified by the intersection of the following curves:

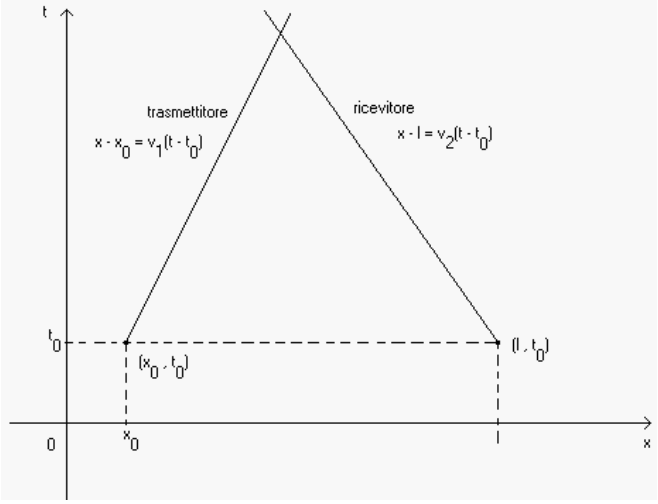

Figure 2.4 - Characteristic curves in the case of transmitter and receiver in motion from [5]

It is also supposed that the transmitter, from the initial instant t_0, emits a sequence of pulses at regular time intervals T_0. As seen above, in a space-time graph, the information associated with the wavefronts will be transmitted according to straight lines whose slope depends on the propagation speed of the supposed wave constant in the middle. Of the two wavefronts only that which advances in the positive direction of space is considered:

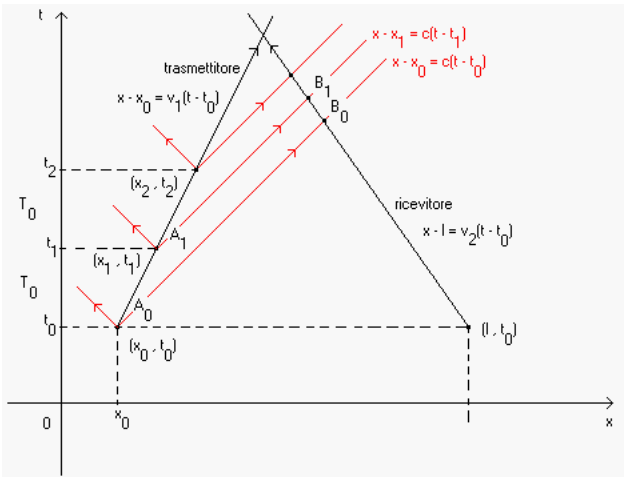

Figure 2.5 - Characteristic curves with positive wavefronts from [5]

The receiver will encounter the waves emitted in the points B_0,B_1 and so on. Therefore, it is taken into account that:

$$t_1 = t_0 + T_0$$

At this point the coordinates of the points are determined B_0 and B_1:

$$\begin{cases} x_{B_0} - l = \mathrm{v}_2(t_{B_0} - t_0) \\ x_{B_0} - x_0 = c(t_{B_0} - t_0) \end{cases} \quad \rightarrow \quad (c - \mathrm{v}_2)(t_{B_0} - t_0) = l - x_0 \quad \rightarrow \quad t_{B_0} = t_0 + \frac{l - x_0}{c - \mathrm{v}_2}$$

$$\begin{cases} x_{B_1} - x_1 = c(t_{B_1} - t_1) = c(t_{B_1} - t_0 - T_0) = c(t_{B_1} - t_0) - cT_0 \\ x_{B_1} - l = \mathrm{v}_2(t_{B_1} - t_0) \end{cases} \quad \rightarrow \quad t_{B_1} = t_0 + \frac{cT_0 + l - x_1}{c - \mathrm{v}_2}$$

Defining T the difference between t_{B_1} and t_{B_0}:

$$T = t_{B_1} - t_{B_0} = t_0 + \frac{cT_0 + l - x_1}{c - \mathrm{v}_2} - t_0 - \frac{l - x_0}{c - \mathrm{v}_2} = \frac{cT_0 + x_0 - x_1}{c - \mathrm{v}_2}$$

From the path of the emitter evaluated in (x_1, t_1), you can write:

$$x_1 - x_0 = \mathrm{v}_1(t_1 - t_0) \quad \rightarrow \quad x_1 - x_0 = \mathrm{v}_1(T_0) \quad \rightarrow \quad x_0 - x_1 = -\mathrm{v}_1(T_0)$$

then you will have:

$$T = t_{B_1} - t_{B_0} = \frac{cT_0 - \mathrm{v}_1 T_0}{c - \mathrm{v}_2} = T_0 \frac{c - \mathrm{v}_1}{c - \mathrm{v}_2}$$

T represents the apparent wave period perceived by the observer, and is certainly different from the initial wave period T_0 emitted by the transmitter. Finally, in case the transmitter is stopped, you will have:

$$\mathrm{v}_1 = 0 \quad ; \quad T = T_0 \frac{c}{c - \mathrm{v}_2}$$

The same apparent variation can be seen by passing to the frequencies and then relating the observer's speed and frequency.

3. SYSTEM COMPONENTS

The basic configuration of an LDA system includes: a continuous wave laser, a transmission optic, a receiving optic, a signal conditioning block, a signal processor and finally inseminating particles.

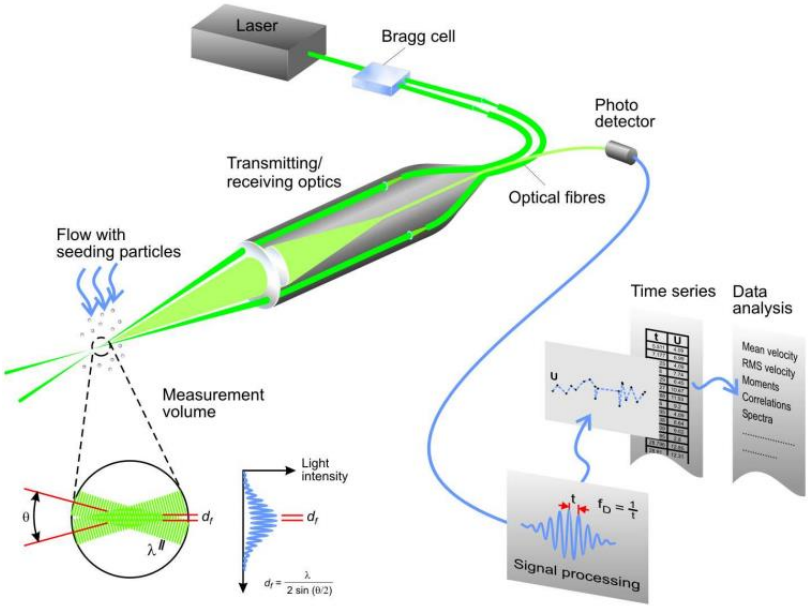

Figure 3.1 - Basic components of an LDA system [6]

In a laser (Light Amplification by Stimulated Emission of Radiation) two main physical phenomena are involved: the stimulated emission that leads to a high degree of monochromatic light and the amplification of the radiation in an optical resonator that ensures a high power density and high consistency then a laser beam that does not diverge. Normally the light passing through a material is absorbed by the material itself, that is, it gives energy to the atoms, because it finds them in a low energetic state, If, however, the atoms are excited with an external energy source, the probability of the stimulated emission increases and therefore a laser light is emitted.

The transmission optics includes a beam divider (Bragg cell) and a focus lens. The Bragg cell consists of a piezoelectric crystal, whose vibration generates acoustic waves that interact with the laser beam. At the exit of the Bragg cell there are two beams of equal intensity: one not deflected having the original frequency f_b and the other deflected having a shifted frequency of a quantity f_{sh}, Both are focused into fiber optics and transported to a probe. Joints in the probe parallel beams are focused in the focusing lens to intersect in the measuring volume.

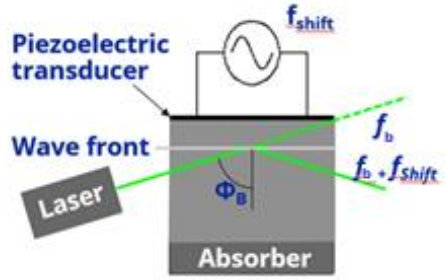

Figure 3.2 - Scheme of operation of a Bragg cell [6]

The receiving optics includes a focusing lens, an interference filter and a photoreceiver. The diffused light is collected by a receiver lens and then focused on a photoreceiver, but before reaching its surface it passes through an interference filter that transmits only the desired wavelength and removes the

noise determined by ambient light, finally, the photoreceiver converts the light intensity into an electrical signal that is easier to handle.

The conditioning block and the signal processor (which will be better discussed later) are used to amplify and filter the signal in order to determine the Doppler frequency f_D and therefore, for the reasons discussed below, the velocity of each particle.

The choice of inseminating particles is of fundamental importance to obtain an accurate measurement, since the particle must not be substantially too large and heavy, otherwise its inertia would be such as to prevent it from following the flow line perfectly, nor too small to go unnoticed by the optical receiver in order to disperse the light adequately. In addition, it is also required that the inseminator is distributed in the most homogeneous way possible since instead a localized insemination could generate a falsified measure of the local flow velocity.

4. LASER DOPPLER ANEMOMETRY

In chapter 2 it was said that the Doppler effect accompanies any movement of the transmitter (source) or receiver (observer) within the wave propagation. In the case of Laser Doppler anemometry the nature of the waves is clearly electromagnetic and the propagation speed is the speed of light in the medium c. The technique is schematically illustrated in figure 4.1:

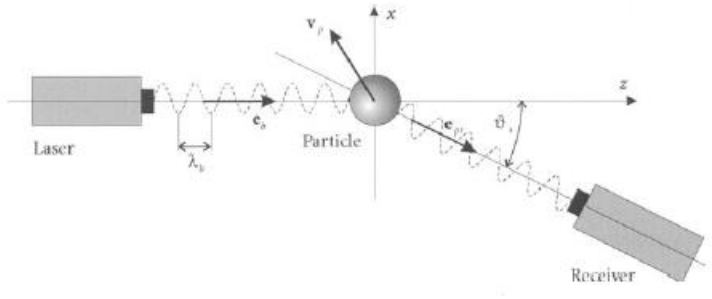

Figure 4.1 - Scheme for the application of the Doppler effect in the LDA technique from [1]

An electromagnetic wave of frequency f_P and wavelength λ_p, emitted by a moving transmitter (a particle) with speed v_P, will be compressed in the direction of motion and expanded in the opposite direction. This results in a variation in the wavelength and frequency perceived by a stationary receiver (figure 4.2b):

$$\begin{cases} \lambda_r = \dfrac{c}{f_p} - \dfrac{\mathbf{v_p} \cdot \boldsymbol{e_{pr}}}{f_p} = \lambda_p - \dfrac{\mathbf{v_p} \cdot \boldsymbol{e_{pr}}}{c/\lambda_p} = \lambda_p \left(1 - \dfrac{\mathbf{v_p} \cdot \boldsymbol{e_{pr}}}{c}\right) \\ f_r = {}^{c}/_{\lambda_r} = \dfrac{c}{\lambda_p \left(1 - \dfrac{\mathbf{v_p} \cdot \boldsymbol{e_{pr}}}{c}\right)} = \dfrac{f_p}{1 - \dfrac{\mathbf{v_p} \cdot \boldsymbol{e_{pr}}}{c}} \end{cases}$$

$$(\text{ if } \mathbf{v_p} \cdot \boldsymbol{e_{pr}} > 0 \quad \rightarrow \quad f_r \uparrow ; \ \lambda_r \downarrow)$$

The frequency f_P and wavelength λ_p perceived by a moving receiver (a particle) in motion with speed v_P compared to a stationary transmitter (a laser) having wavelength λ_b and frequency f_b are (Figure 4.2a):

$$\begin{cases} \lambda_p = \dfrac{\lambda_b}{1 - \dfrac{\mathbf{v_p} \cdot \boldsymbol{e_b}}{c}} = \dfrac{\lambda_b}{\dfrac{c - \mathbf{v_p} \cdot \boldsymbol{e_b}}{c}} \\ f_p = f_b \left(1 - \dfrac{\mathbf{v_p} \cdot \boldsymbol{e_b}}{c}\right) = f_b \left(\dfrac{c - \mathbf{v_p} \cdot \boldsymbol{e_b}}{c}\right) = \dfrac{c - \mathbf{v_p} \cdot \boldsymbol{e_b}}{\lambda_b} = f_b - \dfrac{\mathbf{v_p} \cdot \boldsymbol{e_b}}{\lambda_b} \end{cases}$$

$$(\text{ se } \mathbf{v_p} \cdot \boldsymbol{e_b} > 0 \quad \rightarrow \quad f_p \downarrow ; \ \lambda_p \uparrow)$$

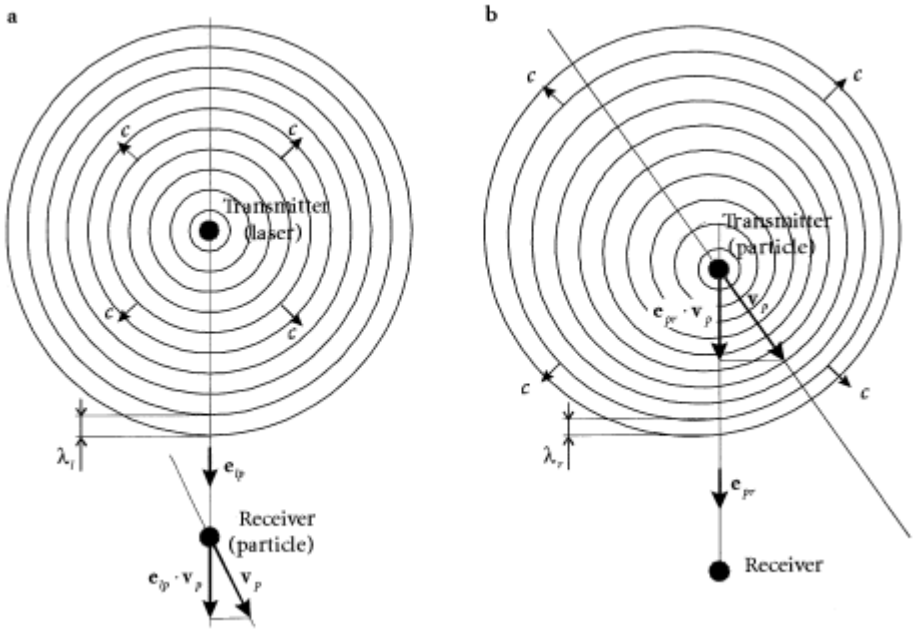

Figure4.2a,b-Doppler effect.a Stationary transmitter and receiver in motion,b Transmitter moving and receiver stationary from [1]

In the Laser Doppler technique the particle in motion assumes the role of both receiver and transmitter so the Doppler effect is called into question twice, once when the laser light of the stationary transmitter, characterized by the wavelength λ_b and frequency f_b (b...*beam*) affects the moving target-particle and once when the light is scattered with wavelength λ_p and frequency f_p (p...*particle*) from the particle itself. Thus, the light detected by a stationary receiver will have a frequency f_r (r...*receiver*):

$$f_r = f_b \frac{1 - \frac{\mathbf{v_p} \cdot \boldsymbol{e_b}}{c}}{1 - \frac{\mathbf{v_p} \cdot \boldsymbol{e_{pr}}}{c}}$$

since $|\mathrm{v}_P| << c$ and then $|\mathrm{v}_P|/c << 1$, there f_r can be rewritten as follows:

$$f_r = f_b \frac{1 - \frac{\mathbf{v_p} \cdot \boldsymbol{e_b}}{c}}{1 - \frac{\mathbf{v_p} \cdot \boldsymbol{e_{pr}}}{c}} \cdot \frac{1 + \frac{\mathbf{v_p} \cdot \boldsymbol{e_{pr}}}{c}}{1 + \frac{\mathbf{v_p} \cdot \boldsymbol{e_{pr}}}{c}} = f_b \frac{\left(1 - \frac{\mathbf{v_p} \cdot \boldsymbol{e_b}}{c}\right)\left(1 + \frac{\mathbf{v_p} \cdot \boldsymbol{e_{pr}}}{c}\right)}{\left[1 - \left(\frac{\mathbf{v_p} \cdot \boldsymbol{e_{pr}}}{c}\right)^2\right]}$$

$$f_r \approx f_b \left(1 - \frac{\mathbf{v_p} \cdot \boldsymbol{e_b}}{c}\right)\left(1 + \frac{\mathbf{v_p} \cdot \boldsymbol{e_{pr}}}{c}\right) = f_b \left(1 + \frac{\mathbf{v_p} \cdot \boldsymbol{e_{pr}}}{c} - \frac{\mathbf{v_p} \cdot \boldsymbol{e_b}}{c} - \left(\frac{\mathbf{v_p} \cdot \boldsymbol{e_b}}{c} \cdot \frac{\mathbf{v_p} \cdot \boldsymbol{e_{pr}}}{c}\right)\right) \approx$$

$$f_b + \frac{\mathbf{v_p} \cdot (\boldsymbol{e_{pr}} - \boldsymbol{e_b})}{\lambda_b}$$

The second term of the last equation is called Doppler frequency. It allows the measurement of velocity, in fact this quantity, which appears only when the direction of propagation of the incident wave $\boldsymbol{e_b}$ and shot $\boldsymbol{e_{pr}}$ differ, is directly proportional to the velocity of the particle $\mathbf{v_p}$. Typically the Doppler frequency is too small (<10^8 Hz) compared to the laser beam (10^{14} Hz) to be solved with optical instruments. For this reason, conventional optical configurations work with two scattered waves each of which exhibits a Doppler frequency or alternatively a Laser beam acts as a reference beam and is mixed to the wave scattered by process of optical Heterodyne, which converts the signal into one more easily manageable by optical instruments.

There are numerous alternatives to implement such systems. For example, using only one incident laser beam, the following configurations can be made (figure 4.3a and 4.3b):

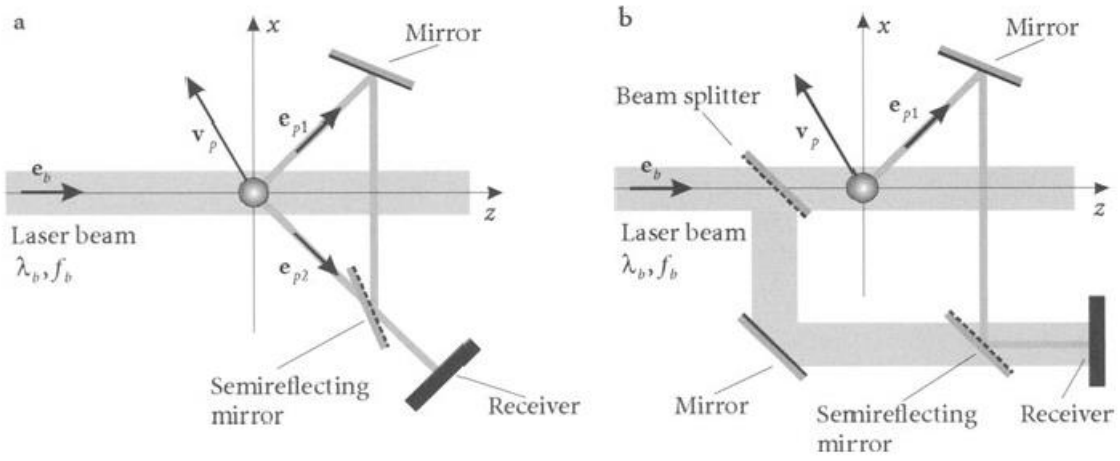

Figure 4.3a,b - Optical configuration with single laser incident system. a Dual-scattered-wave configuration, b One-reference-beam/one-scattered-wave configuration from [1]

In figure 4.3a the "dual-scattered-wave" configuration is illustrated while in figure 4.3b that "one-reference-beam/one-scattered-wave". In both the Doppler frequency or in this case more properly the Doppler deviation f_D is obtained through the mix of the frequency waves f_1 and f_2 on the photoreceiver. For one-beam configuration, the deviation frequencies are obtained as follows:

- dual-scattered-wave *(Figure 4.3a):*

$$f_1 = f_b + \frac{\mathbf{v_p} \cdot (\boldsymbol{e_{p1}} - \boldsymbol{e_b})}{\lambda_b} \quad ; \quad f_2 = f_b + \frac{\mathbf{v_p} \cdot (\boldsymbol{e_{p2}} - \boldsymbol{e_b})}{\lambda_b}$$

$$f_D = f_2 - f_1 = \frac{\mathbf{v_p} \cdot (\boldsymbol{e_{p2}} - \boldsymbol{e_{p1}})}{\lambda_b}$$

- one-reference-beam/one-scattered-wave *(Figure 4.3b):*

$$f_1 = f_b + \frac{\mathbf{v_p} \cdot (\boldsymbol{e_{p1}} - \boldsymbol{e_b})}{\lambda_b} \quad ; \quad f_2 = f_b$$

$$f_D = f_2 - f_1 = \frac{\mathbf{v_p} \cdot (\boldsymbol{e_b} - \boldsymbol{e_{p1}})}{\lambda_b}$$

The measuring volume is defined in both cases using a certain opening on the receiver, in this way a virtual measuring volume is obtained (seen only by the receiver). These systems are not widely used because the small aperture, required to reduce the measuring volume, also leads to a high reduction of the detected light intensity and because the Doppler deviation f_D depends on the location of the detector.

A more widely used configuration is based on two incident waves (figure 4.4a and 4.4b):

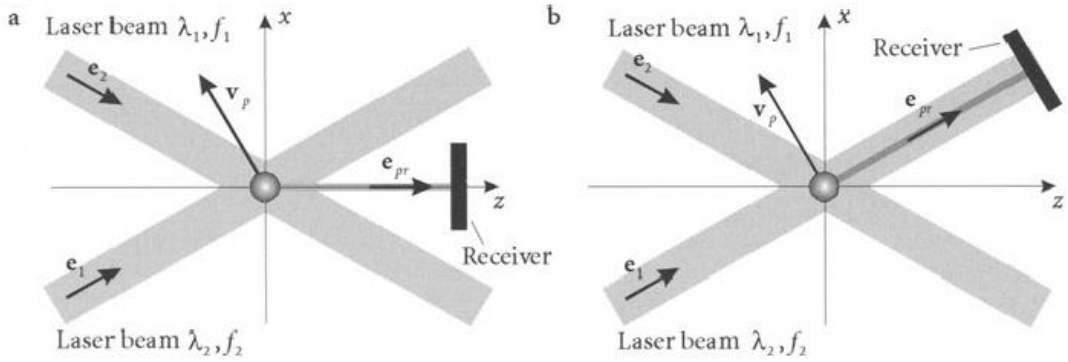

Figure 4.4a,b - Optical configuration with two incident rays system. a Classic dual-beam configuration, b Reference-dual-beam configuration from [1]

Figure 4.4a shows a "classic dual-beam" configuration in which a "real" measuring volume is determined at the intersection of two incident laser beams and the scattered waves are detected by a single photoreceiver. In this case the Doppler f_D deviation is:

$$f_1 = f_b + \frac{\mathbf{v_p} \cdot (\boldsymbol{e_{pr}} - \boldsymbol{e_1})}{\lambda_b} \quad ; \quad f_2 = f_b + \frac{\mathbf{v_p} \cdot (\boldsymbol{e_{pr}} - \boldsymbol{e_2})}{\lambda_b}$$

$$f_D = f_2 - f_1 = \frac{\mathbf{v_p} \cdot (\boldsymbol{e_1} - \boldsymbol{e_2})}{\lambda_b}$$

In figure 4.4b instead, the "reference-dual-beam" configuration is shown, in which the photoreceiver is positioned directly along the path of one of the two laser beams ($\boldsymbol{e_{pr}} = \boldsymbol{e_1}$). In this case the Doppler f_D deviation will be:

$$f_1 = f_b \quad ; \quad f_2 = f_b + \frac{\mathbf{v_p} \cdot (\boldsymbol{e_{pr}} - \boldsymbol{e_2})}{\lambda_b} \quad ; \quad \boldsymbol{e_{pr}} = \boldsymbol{e_1}$$

$$f_D = f_2 - f_1 = \frac{\mathbf{v_p} \cdot (\boldsymbol{e_1} - \boldsymbol{e_2})}{\lambda_b}$$

It is important to note that for dual-beam configurations, the Doppler offset is independent of the receiver position. In Figure 4.4 if θ is given the angle of intersection between the two rays, the Doppler deviation frequency detected by the photodetector, as clarified by Figure 4.5, will be given by:

$$f_D = \frac{2\sin{}^{\theta}/_{2}}{\lambda_b}\left|\mathbf{v_p}\right|\cos\alpha = \frac{2\sin{}^{\theta}/_{2}}{\lambda_b}\mathrm{v}_{p\perp}$$

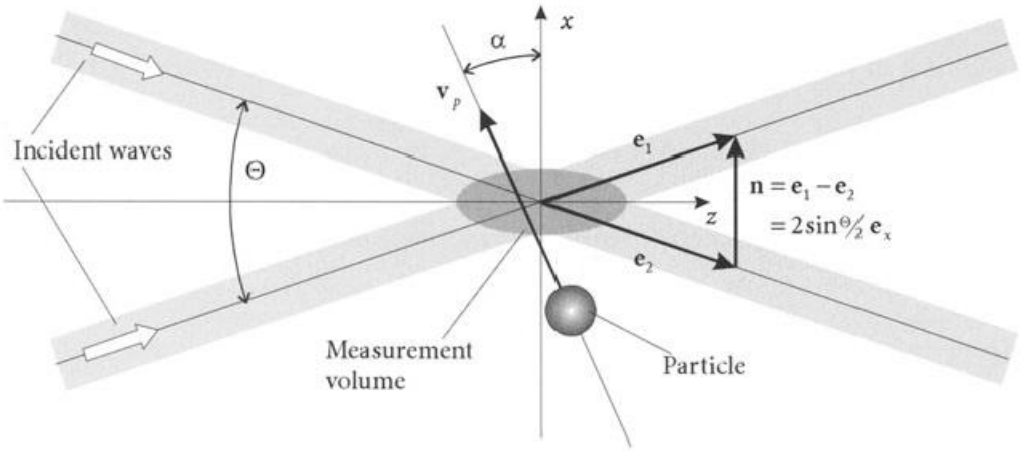

Figure 4.5 - Vector relations to derive the frequency Doppler from [1]

The last relationship represents the characteristic of the instrument. Observing this function, the following considerations are made:

- The instrument measures the velocity component perpendicular to the bisector between the two laser beams;
- Speed measurement does not depend on receiver position;
- The equation is linear algebraic and the offset Doppler is directly proportional to the velocity component;
- The coefficient of sensitivity, having dimensions inverse to those of a length, depends only on the optical parameters of the configuration used. In fact, choosing the type of laser (λ_b) and setting the angle between the two incident beams (θ), the coefficient of sensitivity is automatically determined. So the instrument does not need any calibration.

5. PHYSICAL PRINCIPLE OF DOPPLER LASER ANEMOMETRY

For a more detailed explanation of the physical principle behind Laser Doppler anemometry, in the case of inseminating particles of very small diameter ($d_p << \lambda_b$), you can refer to the interference fringe model. This model is essentially based on the spatial energy density in the measuring volume as will be explained below.

A plane and homogeneous electromagnetic wave (ie electric and magnetic field, perpendicular to each other, always oscillate along the same directions) can be described through the following electric field vector:

$$\boldsymbol{E} = \boldsymbol{e_E} E_0 \cos(\omega_b t - \boldsymbol{k_b} \cdot \boldsymbol{r} + \varphi_b)$$

With the notation of complex numbers you can write:

$$\underline{\boldsymbol{E}} = \boldsymbol{e_E} E_0 \exp[j(\omega_b t - \boldsymbol{k_b} \cdot \boldsymbol{r} + \varphi_b)] = \boldsymbol{e_E} E_0 \{\cos(\omega_b t - \boldsymbol{k_b} \cdot \boldsymbol{r} + \varphi_b) + j \sin(\omega_b t - \boldsymbol{k_b} \cdot \boldsymbol{r} + \varphi_b)\}$$

$$E = Re\{\underline{\boldsymbol{E}}\}$$

Where ωb is pulsation, k_b represents the wave vector in the direction of propagation of the laser having a wave number of $k_b = 2\pi\ \lambda b$, e_E is the bias versor, E_0 the amplitude of the electric field, r is a vector that defines an arbitrary point in space and finally φ_b is the phase of the electromagnetic wave at the origin and time $t = 0$. If the two incident laser beams are of equal intensity E_0, with a polarization e_y perpendicular to the x-z plane where the rays lie symmetrically (figura5a and 5b), then the fields of the two rays can be described by:

$$\begin{cases} \underline{E_1} = E_0 \exp\left(j\left[\omega_b t - k_b\left(x \sin {}^{\theta}/_{2} + z \cos {}^{\theta}/_{2}\right) + \varphi_1\right]\right) \\ \underline{E_2} = E_0 \exp\left(j\left[\omega_b t - k_b\left(-x \sin {}^{\theta}/_{2} + z \cos {}^{\theta}/_{2}\right) + \varphi_2\right]\right) \end{cases}$$

The electric field in the intersection volume determined by the two laser beams crossing at an angle θ will simply be the overlap of the two fields (figura5c), or:

$$\underline{\boldsymbol{E}} = \underline{\boldsymbol{E_1}} + \underline{\boldsymbol{E_2}} = \left(\underline{E_1} + \underline{E_2}\right) \boldsymbol{e_y}$$

Thus, if the E_1 and E_2 phases are given with A, the following total field is given:

$$\underline{E} = \underline{E_1} + \underline{E_2} = E_0(e^{JA} + e^{JB}) = E_0(\cos A + j \sin A + \cos B + j \sin B)$$

$$= E_0(\cos A + \cos B) + jE_0(\sin A + \sin B)$$

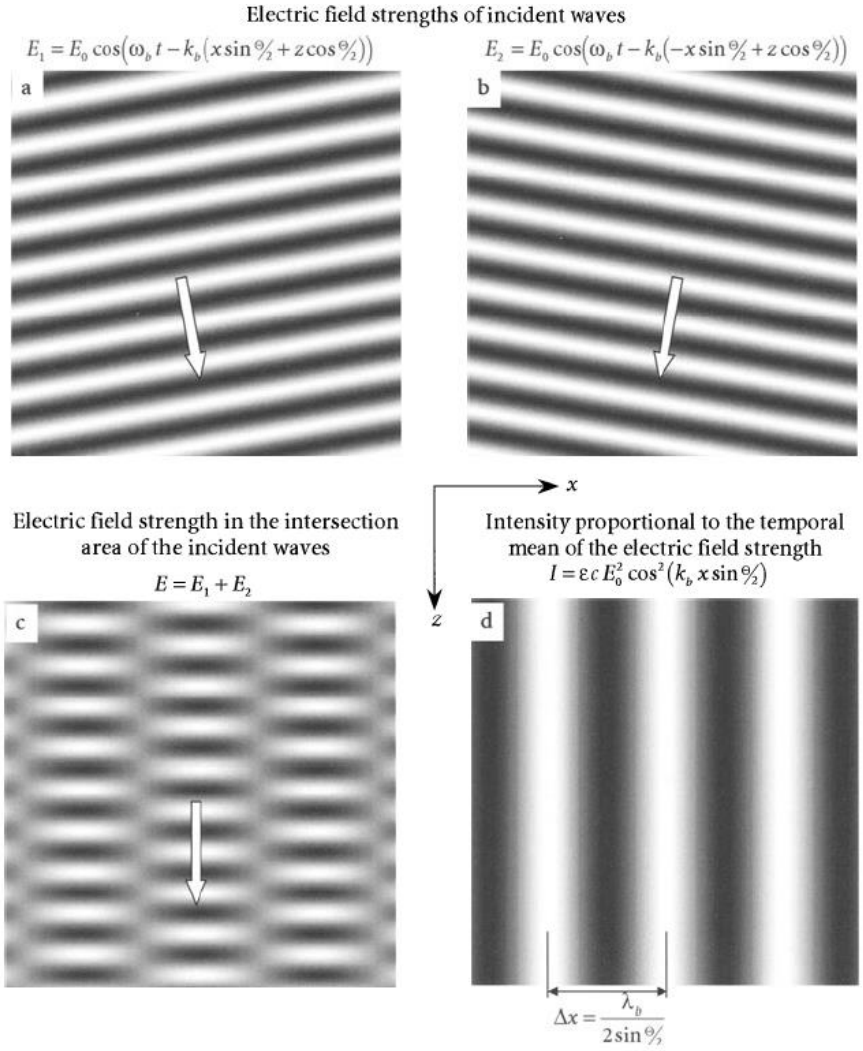

Figure 5a,b,c,d - Generation of an interferometric pattern from two waves homogeneous. a,b Electric field strength of incident waves, c Overlap of electric fields, d Intensity of the total field from [1]

Having defined ε the electrical permittivity and μ the magnetic permeability of the medium, the energy density of the field in the measuring volume can be described by:

$$w = \frac{1}{2}(\varepsilon E^2 + \mu H^2); \quad E = |\underline{\boldsymbol{E}}|; \quad H = |\underline{\boldsymbol{H}}|$$

With **H** vector of magnetic field which, in complex representation, will be:

$$\underline{\boldsymbol{H}} = \boldsymbol{e_H} \sqrt{\frac{\varepsilon}{\mu}} E_0 \exp[j(\omega_b t - \boldsymbol{k_b} \cdot \boldsymbol{r} + \varphi_b)]$$

so you have:

$$w = \frac{1}{2}(\varepsilon E^2 + \mu H^2) = \frac{1}{2}(\varepsilon E^2 + \varepsilon E^2) = \varepsilon E^2$$

Namely electric and magnetic field contain the same amount of energy.

It can be demonstrated that the energy density in the measuring volume takes the following form:

$$w = 4\varepsilon {E_0}^2 \underbrace{\cos^2\left(k_b x \sin {\theta}/{2} - \frac{\varphi_1 - \varphi_2}{2}\right)}_{\text{Modulating function}} \underbrace{\cos^2\left(\omega_b t - k_b z \cos {\theta}/{2} + \frac{\varphi_1 + \varphi_2}{2}\right)}_{\text{carrier function}}$$

This quantity can be interpreted as a wave propagating in the z-direction with an amplitude modulated along the x-direction equal to the following quantity:

$$4\varepsilon {E_0}^2 \cos^2\left(k_b x \sin {\theta}/{2} - \frac{\varphi_1 - \varphi_2}{2}\right)$$

The intensity of the electromagnetic wave as defined is obtained by averaging over a period of energy density:

$$I = c\langle w(t)\rangle = \varepsilon c\langle E^2(t)\rangle \qquad con \qquad \langle f(t)\rangle = \frac{1}{T}\int_0^T f(t)\,dt$$

In the complex form, this is reduced roughly to the multiplication of the total field vector by its complex and conjugate value ($E\,E^*$), and if the phases are equal, that is $\varphi_1 = \varphi_2$, the intensity of the field becomes:

$$I = \frac{\varepsilon c}{2}\underline{E}\cdot\underline{E}^* = \frac{\varepsilon c}{2}[E_0(\cos A + \cos B) + jE_0(\sin A + \sin B)]\cdot[E_0(\cos A + \cos B) - jE_0(\sin A + \sin B)] =$$

$$\frac{\varepsilon c}{2}{E_0}^2\{(\cos A + \cos B)^2 + (\sin A + \sin B)^2\} = \frac{\varepsilon c}{2}{E_0}^2(2 + 2(\cos(B - A)) =$$

$$\frac{\varepsilon c}{2}2{E_0}^2\left(1 + \cos^2\left(\frac{B-A}{2}\right) - \sin^2\left(\frac{B-A}{2}\right)\right) = \frac{\varepsilon c}{2}4{E_0}^2\left(\cos^2\left(\frac{B-A}{2}\right)\right) =$$

$$2\varepsilon c{E_0}^2\cos^2\left(k_b x \sin {\theta}/{2}\right) = 2\varepsilon c{E_0}^2\left(\frac{1+\cos\left(2k_b x \sin {\theta}/{2}\right)}{2}\right) =$$

$$\varepsilon c{E_0}^2\left[1 + \cos\left(2k_b x \sin {\theta}/{2}\right)\right]$$

$$\cos(\alpha - \beta) = \cos(\alpha)\cos(\beta) + \sin(\alpha)\sin(\beta)$$

$$\cos\left(\frac{\alpha}{2}\right) = \pm\sqrt{\frac{1 + \cos(\alpha)}{2}}$$

Einfine esplicitado $k_b = 2p\,/\,l_b$, si ottiene: $$I = \varepsilon c{E_0}^2\left[1 + \cos\left(2\pi\frac{2\sin {\theta}/{2}}{\lambda_b}x\right)\right]$$

The spatial dependence of the field intensity in the measurement volume can be interpreted as an interference field with fringes parallel to the y-z plane (figura5d). Fringe spacing is contained in the cosine function argument:

$$\Delta x = \frac{\lambda_b}{2\sin {\theta}/{2}}$$

At this point if in the last equation the coordinate occupied by the particle during the crossing of the measuring volume, or $v_p\ t$, is substituted for the x-position, the:

$$I = \varepsilon c {E_0}^2 \left[1 + \cos\left(2\pi \frac{2\sin {}^{\theta}/_{2}}{\lambda_b} \mathrm{v}_{p\perp} t\right)\right] = \varepsilon c {E_0}^2 [1 + \cos(2\pi f_D t)]$$

The latter equation provides a clear physical interpretation of the principle of operation of the instrument. A small particle of diameter much smaller than the distance between the fringes, passing through it, is as if it were actually sampling the local intensity of the field in the measuring volume. A particle of diameter d_p has an average power of about:

$$P \approx I A_p \approx I \frac{\pi}{4} {d_p}^2$$

And scatter such power in all directions. The scattered wave is modulated in amplitude and has a carrier frequency equal to that of the laser beam. Therefore, an electrical signal $i(t)$ is obtained from the photoreceiver proportional to the intensity of the field crossed by the particle, the amplitude of which is modulated with the frequency f_D:

$$i(t) \sim \varepsilon c {E_0}^2 [1 + \cos(2\pi f_D t)] \quad , \quad f_D = \frac{2\sin {}^{\theta}/_{2}}{\lambda_b} \mathrm{v}_{p\perp}$$

The velocity component perpendicular to the interference fringes v_p is therefore inversely proportional to the period of crossing the fringe T_D:

$$\mathrm{v}_{p\perp} = \frac{\Delta x}{T_D}$$

As mentioned above, for the Doppler laser technique, the fringe model is only valid for small tracer particles complying with the condition $d_p \ll \lambda_b$. This is mainly because only in this specific case the amplitude and phase, or the intensity of the field, can be considered constant along the diameter of the particle. The particle then interacts with the field in the measuring volume and in turn generates a scattered field of intensity proportional to the sum of individual fields. The flux of scattered energy is detected by a photoreceiver. This component averages the power density over time because of its finite response time and integrates the intensity in the space on the detector surface. The electrical signal obtained is directly proportional to the spatial energy density in the measuring volume therefore, the small particle samples in fact the local intensity of the interferometric pattern. For larger particles this model fails because both the phase and amplitude of incident waves vary along the particle diameter (figure5.1).

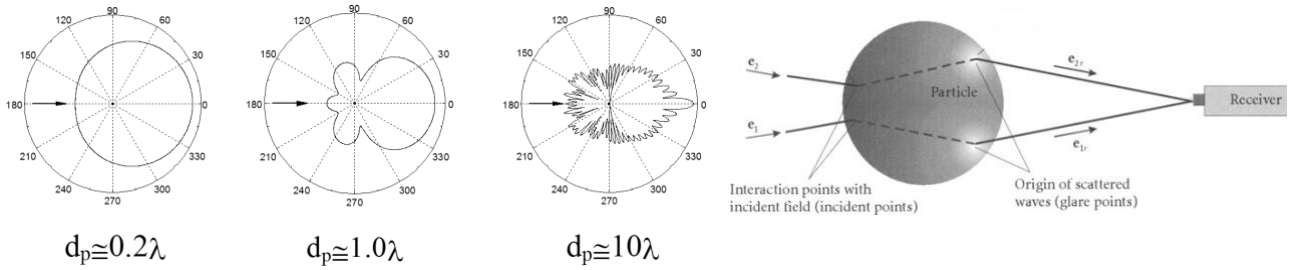

Figure 5.1 - Signal originated in the case of large particles from [6] and [1]

6. DISCRIMINATION OF THE DIRECTION

The optical arrangement, discussed in chapter 4, produces the normal velocity component at the interference fringes; however, its verse is no longer contained in the obtained signal. In fact, two particles moving with equal but opposite velocities through the measuring volume, will generate the same signal on the detector (figure6.1a). The information on the directionality of the motion of the particle is retrieved if two laser beams are used that are incident at different wavelengths (different frequencies). A wavelength shift of one or both laser beams can be achieved by acusto-optical modulators, such as Bragg cells. So if a modulator is mounted in the path of radius 1, the frequency of the radius can be varied by a quantity f_{sh} :

$$f_1 = f_b \pm f_{sh}$$

In the fringe model this corresponds to a movement of the fringes in the direction -x or +x with a constant velocity of $v_{sh} = f_{sh}x$ and therefore the velocity of the particle is measured against a moving reference (Figure 6.1b).

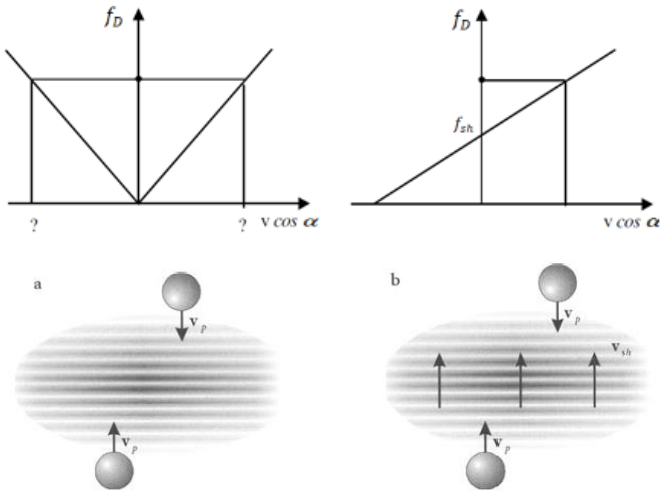

Figure 6.1a,b - Explanation of the frequency-shift technique for directional sensitivity. a Without shift frequency, b with shift frequency from [1] and [2]

In this way the detected Doppler offset will show an offset of its own equal to the f_{sh} frequency. Thus, for a stationary particle the detected signal will have a frequency f_{sh} modulation due to the fact that the fringes are passing through the position occupied by the particle at $f_{sh}\Delta x$ where Δx represents the distance between the fringes. It is easy to guess that instead, a particle that moves in the direction of the fringes, chasing them, will feel a lower Doppler deviation. Conversely, a movement of the particle in opposition to that of the fringes will produce a higher frequency (figure6.2).

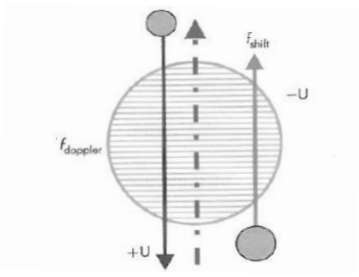

Figure 6.2 - Diagram of relative velocities between particle and fringes from [3]

7. SPATIAL AND TEMPORAL RESOLUTION

In this chapter, attention is paid to the measuring volume and the scattering particles. It must be considered that the distribution of luminous intensity, along a transverse direction with respect to that of propagation of the ray, is in good Gaussian approximation (TEM_{00} - figure 7a) and that this transverse dimension D is of the order of a few tenths of a millimetre (having taken as end the points where the intensity takes a value equal to 1 and 2 times that of the center). As a result, the typical dimensions of the measuring volume (that is, of the "sensitive" element of the LDA system) are approximately (figure 7b):

$$\delta_z = \frac{D}{\sin \theta/2} \quad ; \quad \delta_x = \frac{D}{\cos \theta/2} \quad ; \quad \delta_y = D$$

In other words, the volume lengthens a lot in the z-direction if θ is small. Typically $\theta = 10$, which gives $\delta_z \approx 10D \approx 1\ mm$ and $\delta_x \approx \delta_y \approx D \approx 0.1\ mm$. These are the characteristic dimensions to be used to determine the spatial resolution.

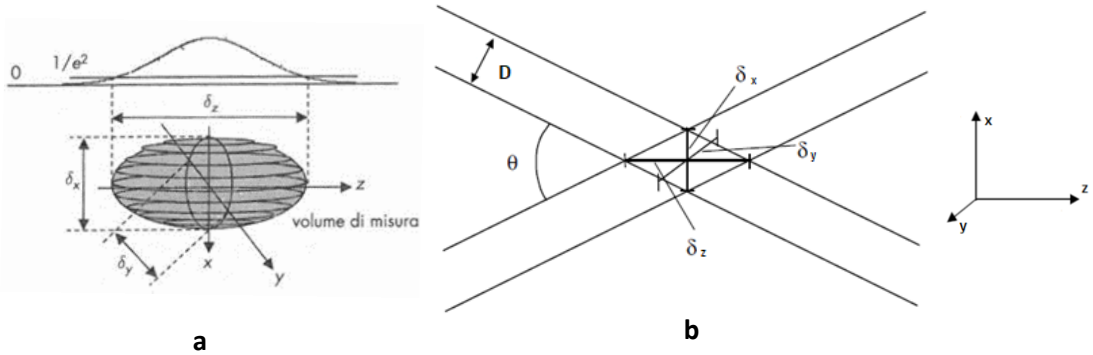

Figure 7a,b -a Laser beam intensity from [3], b Characteristic dimensions of the measurement volume in the LDA technique from [2]

As for the diffusing particles, in water there are usually no big problems (there are, in fact, natural impurities with dimensions of the order of the micrometer), while in air are introduced calibrated spherical particles (water or water bubbles and glycerin smaller than a micron). With such particles a number of data acquired per second equal to more than 1000 is reached and the corresponding time interval (1/1000 s) constitutes the reference time for the temporal resolution.

8. SIGNAL FORM, PROCESSING AND SAMPLING

At this point you can see the typical shape of a signal that you get from an LDA system. From the fringed model, considering that the distribution of the intensity of the light in the measuring volume (as well as on a beam) is roughly that of a normal one (figura8.1b), we deduce that the signal will have a low frequency component of Gaussian type (known as pedestal) with a higher frequency component superimposed (figure 8.1a). The latter contains information on the Doppler deviation and therefore the flow velocity.

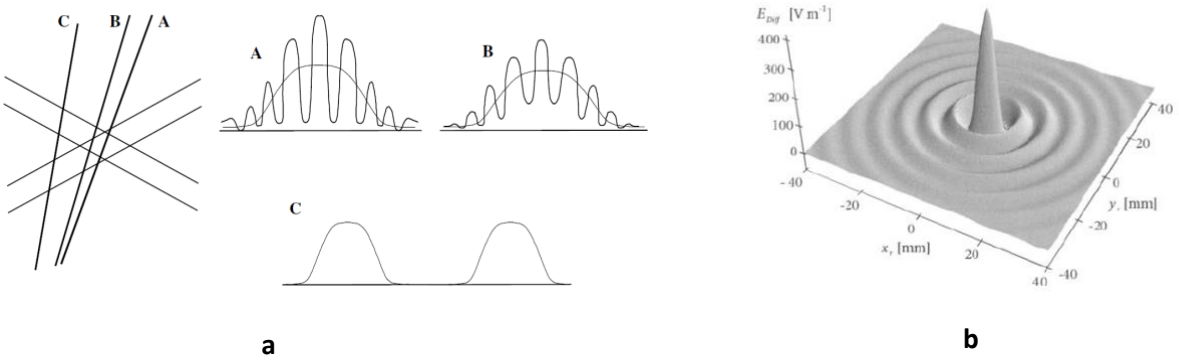

Figure 8.1a,b - a Shape of the Doppler signal resulting in different areas of the measuring volume from [2], b Light intensity distribution in the measuring volume from [1]

In fact, in Chapter 5 it was found that the intensity of the incident light was:

$$I(t) = \varepsilon c {E_0}^2 [1 + \cos(2\pi f_D t)]$$

And that the intensity of diffused light collected by the photoreceiver is proportional to it:

$$i(t) \sim \varepsilon c {E_0}^2 [1 + \cos(2\pi f_D t)]$$

The light intensity detected by the photoreceiver takes the following form:

$$i \approx \frac{8I(t)}{\pi D^2} e^{-\frac{8x^2}{D^2}} = \frac{8I(t)}{\pi D^2} e^{-8\left(\frac{v_{p\perp}}{D}t\right)^2} = \frac{8I(t)}{\pi D^2} e^{-\left(\frac{t}{\tau}\right)^2}$$

Con costante di tempo τ pari a:

$$8\left(\frac{v_{p\perp}}{D}t\right)^2 = \left(\frac{t}{\tau}\right)^2 \quad \rightarrow \quad \sqrt{8}\frac{v_{p\perp}t}{D} = \frac{t}{\tau} \quad \rightarrow \quad \tau = \frac{D}{\sqrt{8}\cdot v_{p\perp}}$$

That is because$v_{p\perp}=\Delta x/T_D=f_D\Delta x$, you have:

$$\tau = \left(\frac{D}{\sqrt{8}\,\Delta x}\right)\frac{1}{f_D}$$

Since the distance between the fringes Δx is much smaller than the width of the laser beam D, it can be deduced that $\tau >> 1/f_D$ and then there will be a low frequency Gaussian component dictated substantially by the intensity distribution of the Laser beam that determines the so-called "pedestal" while the high frequency component due to the Doppler deviation is contained in the cosine argument that appears by explicating the intensity of the field $I(t)$:

$$i(t) \approx \left(\frac{8e^{-\left(\frac{t}{\tau}\right)^2}}{\pi D^2} \right) \varepsilon c {E_0}^2 [1 + \cos(2\pi f_D t)]$$

Pedestal (Gaussian) — high-frequency component

As can also be seen from Figure 8.1a, the signal quality degrades rapidly due to particles passing away from the centre of the measuring volume. In reality, the intensity of the signal spread by the particle depends on the size of the scattering particle, its refractive index (compared to that of the medium), the wavelength and intensity of the incident light and the distance between the particle and the receiver. Figure 8.2 shows that the optimal position of the latter is around the forward direction, coinciding with the direction of propagation of the incident wave ("forward scatter"), but much more often the backward configuration ("backscatter") is used because it is advantageous for the compactness of the system that can thus incorporate in a single unit the components for the transmission and reception of light. It is important to note that, if the two rays do not intersect, it is not possible to obtain any Doppler signal (figure8.1a, caseC) therefore the optical alignment phase is extremely important.

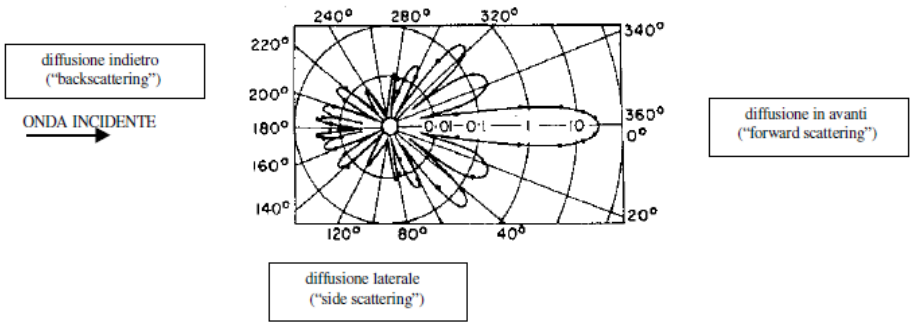

Figure 8.2 - Lobes of radiation intensity spread by a particle and principal directions of diffusion (distance of the lobes is in logarithmic scale) from [2]

The electronic tool used for conditioning and processing the Doppler signal is the component that has undergone the greatest number of updates over time. The first instruments were derived from RADAR technology and operated with a frequency tracking circuit (Tracker) able to follow in real time the changes in frequency Doppler and then speed. The tracker requires a quasi-continuous input, that is generated by a regular succession of particles that pass through the measuring volume seamlessly. This condition occurs easily for fluids such as water where it is easier to have high concentrations of tracers (since they are already naturally present) and for this reason the first applications of the instrument mainly concerned hydraulic experimentation. A digital processor (Counter) based on a counter was later introduced that could measure the number of Doppler signal periods of a single particle in the time unit.

The advantage over its predecessor is that the measurement can take place in a discontinuous way because the counter is activated by the arrival of a signal of amplitude greater than a certain threshold, associated with the passage of a single particle. This procedure is particularly suitable for gas flows where the concentration of tracers is less high and their distribution over time is completely random. However, the counter is particularly sensitive to the noise in the signal (due to threshold levels) and therefore requires careful adjustment of the amplification and air conditioning filters. The presence of noise in the Doppler signal derives from numerous causes of electronic (thermal noise), optical (laser beam quality, background brightness, reflected light) and mechanical (vibration).

The latest development in terms of processors is associated with the introduction of circuits dedicated to frequency measurement using FFT procedures, called spectral analysis processors. Modern instruments are able to perform this operation in real time on the Doppler signal generated by every single particle (figure8.3), despite the shortness of the sampling time (equal to the transit time) and the limited number of acquirable samples (between 16 and 256). The signal analysis procedures are very sophisticated and involve a translation to lower frequencies to reduce the sampling frequency, a verification that the signal is generated by a single particle, a measurement validation as a function of the ratio of the highest peak of the spectrum to any secondary peaks or background and spectrum interpolation procedures to define the Doppler offset with the highest resolution. Fourier analysis is the most accurate numerical procedure to determine the dominant frequency in a signal contaminated by high noise. The electronics of such processors is completely digital and the speed is such as to allow the acquisition of even 10^5 speed measurements per second with very good accuracy.

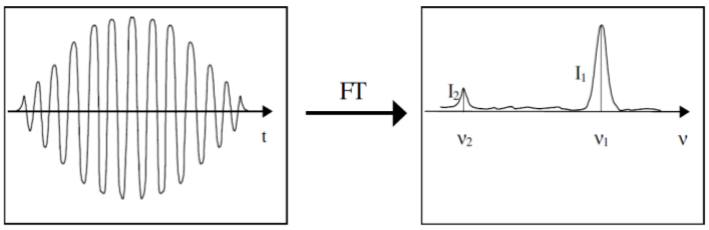

Figure 8.3 - Spectral analysis of an LDA signal from [2]

Downstream of each of the previous signal processors, the values of the measured speed component are available at different times. However, unlike the hot wire anemometer, these speed data are not related to consecutive instants spaced regularly; depending on the random arrival of the tracer particles in the measuring volume, the data is separated by equally random time intervals (except for the Tracker which provides a continuous analog signal). We therefore talk about randomly sampled signals. As can be seen from Figure 8.4, this random sampling can in some cases be an advantage (that is, there is closer information than in the regular case) and in others a disadvantage (more distant information).

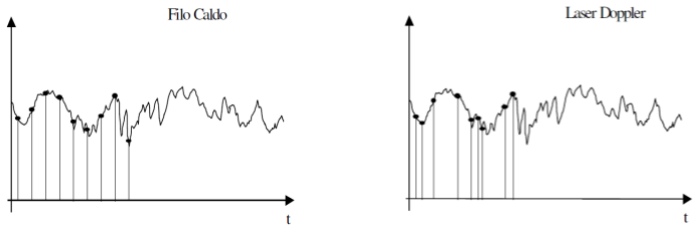

Figure 8.4 - Equispaced and not equispaced (random) sampling by [2]

9. ACCURACY OF THE LDA SYSTEM

Another problem of the LDA technique is related to the observation of an event (the passage of a particle in the measuring volume) that has a finite duration in time and in trying to determine the frequency of the signal. The consequence is that the measurement of the Doppler deviation is intrinsically from an error related to the finite time interval (figure9.1), and indicating with τ_t the transit time you have:

$$\delta v = u_f \approx \frac{1}{\tau_t}$$

This error affects the temporal history with the formation of a band around the measured value that in fact constitutes a noise called "enlargement noise" (or "broadening noise"). In fact, in the frequency domain the signal assumes, with respect to a signal of a hot wire anemometer (HWA), the spectrum given in figure9.2.

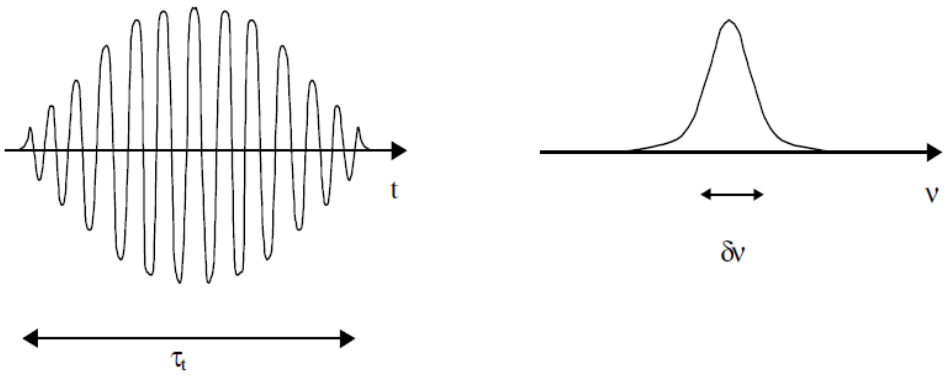

Figure 9.1 - Finite transit time and spectral amplitude from [2]

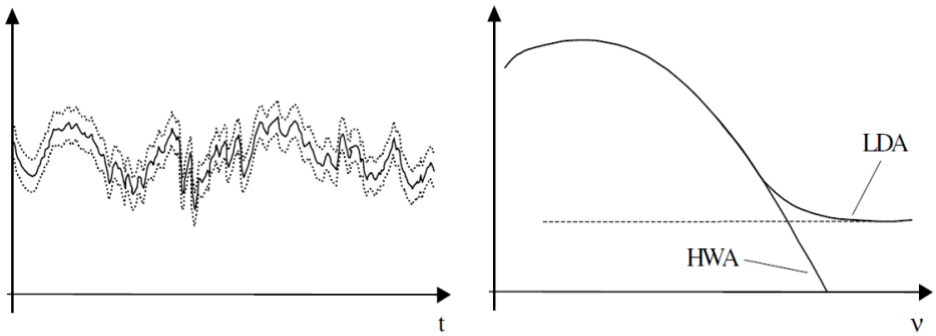

Figure 9.2 - Temporal trend with noise of widening and resulting spectrum from [2]

To get an overall idea of the error that is made in the calculation of the speed with the LDA technique, we derive the overall uncertainty in the hypothesis of unrelated quantities:

$$v_{p\perp} = \Delta x \, f_D = \frac{\lambda_b \; f_D}{2 \sin {}^{\theta}/_{2}}$$

$$\left(\frac{u_{v_{p\perp}}}{v_{p\perp}}\right)^2 = \frac{1}{{v_{p\perp}}^2}\left[\left(\frac{\partial v_{p\perp}}{\partial \Delta x} u_{\Delta x}\right)^2 + \left(\frac{\partial v_{p\perp}}{\partial f_D} u_{f_D}\right)^2\right] = \left(\frac{u_{\Delta x}}{\Delta x}\right)^2 + \left(\frac{u_{f_D}}{f_D}\right)^2$$

oppure

$$\left(\frac{u_{v_{p\perp}}}{v_{p\perp}}\right)^2 = \frac{1}{{v_{p\perp}}^2}\left[\left(\frac{\partial v_{p\perp}}{\partial \lambda_b} u_{\lambda_b}\right)^2 + \left(\frac{\partial v_{p\perp}}{\partial f_D} u_{f_D}\right)^2 + \left(\frac{\partial v_{p\perp}}{\partial \sin {}^{\theta}/_{2}} u_{\sin {}^{\theta}/_{2}}\right)^2\right]$$

$$= \left(\frac{u_{\lambda_b}}{\lambda_b}\right)^2 + \left(\frac{u_{f_D}}{f_D}\right)^2 + \left(\frac{u_{\sin {}^{\theta}/_{2}}}{\sin {}^{\theta}/_{2}}\right)^2$$

Whereas the error on the wavelength u_{λ_b} is generally negligible, you can write:

$$\left(\frac{u_{v_{p\perp}}}{v_{p\perp}}\right)^2 \approx \left(\frac{u_{f_D}}{f_D}\right)^2 + \left(\frac{u_{\sin {}^{\theta}/_{2}}}{\sin {}^{\theta}/_{2}}\right)^2$$

The other two terms represent the error on the angle of intersection between the rays and the error (examined above) on the determination of the frequency. Overall, considering the use of a processor based on spectral analysis, there is an error less than 1%.

10. CONSIDERATIONS ON TRACER PARTICLES

As already mentioned, the Doppler laser technique more correctly measures one or more speed components of the individual tracer particles that cross the measuring volume. To become an anemometer or a measuring instrument of the speed of the continuous phase, Gaseous or liquid, the particles must properly follow the fluid both in its average motion and in turbulent fluctuations up to the highest frequencies associated with the smallest spatial scales. The dynamic behaviour of a particle immersed in a moving fluid is studied to ensure this is the case and to select the most suitable tracers. The analysis is simplified by the following assumptions:

- spherical particles;
- Negligible interaction between particles;
- absence of external forces;
- low relative velocity between particle and fluid (negligible flow);
- high particle density to fluid density ratio.

Consider then the balance between the inertia force of the particle and the viscous drag force:

$$\frac{\pi\, {d_p}^3}{6}\rho_p \frac{dU_p}{dt} = \frac{C_D}{2}\frac{\pi\, d_p^2}{4}\rho_f \left(U_f - U_P\right)^2$$

in which the subscript "p" refers to the particle and the subscript "f" to the fluid, while C_D is the Drag coefficient of the particle.

For the condition of low relative velocity between particle and fluid and small particles, the following condition is considered plausible:

$$Re_p = \frac{\rho_f \left|U_f - U_p\right| d_P}{\mu_f} < 1$$

So, you assume the Stokes regime: $C_D = \frac{24}{Re_p}$

And substituting the coefficient of resistance in the equation of the balance is obtained:

$$\frac{\pi\, {d_p}^3}{6}\rho_p \frac{dU_p}{dt} = 3\pi\mu_f d_p \left|U_f - U_p\right|$$

The equation of the motion of the particle is differential of the first order namely:

$$\underbrace{\left(\frac{\pi\, {d_p}^3}{6}\rho_p\right)}_{a_1}\frac{dU_p}{dt} + \underbrace{\left(3\pi\mu_f d_p\right)U_p}_{a_0} = \underbrace{\left(3\pi\mu_f d_p\right)U_f}_{b_0}$$

The ability of the particle to correctly follow the motion of the fluid depends only on its relaxation time (time constant) equal to the ratio of the coefficients a_1 and a_0, that is:

$$\tau_p = \frac{\rho_p d_p^2}{18\mu_f}$$

While the static sensitivity is equal to the ratio of b_0 and a_0: $k_p = \frac{3\pi\mu_f d_p}{3\pi\mu_f d_p} = 1$

The particle has a behavior similar to that of a low pass filter and therefore you can find the transfer function module simply as:

$$M = \frac{q_o}{q_i} = \frac{k}{\sqrt{1+(\omega\tau)^2}} \quad \rightarrow \quad \frac{U_p}{U_f} = \frac{1}{\sqrt{1+\omega^2\tau_p^2}}$$

with ω=$2\pi f$ frequency of turbulent fluid fluctuations.

The previous report can be rewritten by highlighting the cutting frequency (cut-off) as a function of the time constant and the ratio U_p/U_f:

$$f_c = \frac{1}{2\pi\tau_p}\sqrt{\frac{1}{\left(\frac{U_P}{U_f}\right)^2} - 1}$$

If a maximum deviation of 1% so at least U_p/U_f=0.99, there is: $f_C = \frac{0.0227}{\tau_P}$

The time constant depends on the size of the particles so they must be small to ensure a system with an τ_P lower and thus allow the detection of turbulence associated with higher frequencies. The dependence of the diameter of the cutting frequency:

$$d_P < \left[\frac{18\mu_f}{2\pi\rho_P f_c}\sqrt{\frac{1}{\left(\frac{U_p}{U_f}\right)^2} - 1}\right]^{1/2}$$

This report provides a selection criterion on tracer particles for a given test condition, according to the required accuracy and the maximum frequency of the turbulent phenomena to be detected. Monodisperse particles (of the same size) are preferred to have uniformity of behaviour; therefore, the naturally present particulates are removed from the fluid, as they have uncontrollable particle size dispersion. Sub-micrometric particles ensure adequate dynamic responses comparable to those of a constant temperature wire anemometer (CTA). The lower limit for particle size is determined by the requirement that particles are insensitive to molecular thermal agitation motion and that they provide a light signal amplitude greater than the sensitivity of the photoreceiver-amplifier system.

Below are the cutting frequencies guaranteed by some of the most common particles according to their diameter:

Fluido	Frequenza	Particella [μm]			
	f_c [kHz]	TiO_2 $\rho = 3900\,[kg\,m^{-3}]$	Sfere di vetro $\rho = 2600\,[kg\,m^{-3}]$	Acqua $\rho = 1000\,[kg\,m^{-3}]$	Olio $\rho = 912\,[kg\,m^{-3}]$
Aria	1	1.25	1.5	2.5	2.6
	2	0.9	1.1	1.8	1.8
	5	0.56	0.69	1.1	1.2
	10	0.4	0.5	0.78	0.82

Table A - Maximum tracer particle diameters for $\frac{U_p}{U_f} \geq 0.99$ from [3]

Particle transport dynamics may introduce a systematic error in the determination of statistical quantities (mean value, standard deviation, probability density of fluid velocity). The error is caused by the fact that in a turbulent flow with large speed fluctuations the probability of transit of particles, even if distributed homogeneously in the fluid, is linked to the velocity module U by the relationship:

$$\dot{n} = \eta NUA$$

In which $\dot{n}$ is the number of particles passing through the measuring volume in the unit of time, N is the volumetric concentration of particles in the flow, A is the section of the measuring volume normal to the mean flow direction, η is the percentage of particles that provide a valid signal. Therefore, when the velocity is higher, more particles pass and then on a sample of M measures there will be more at the highest speeds and therefore the average value will be overestimated (according to the arithmetic mean). This effect will be all the greater the larger the turbulent fluctuations and will introduce an error that is necessary to minimize with some corrective criterion. This is a problem that has received several solutions based on the introduction of a weight factor to be attributed to each measure in the evaluation of the statistical parameters, for which we will estimate the average speed on a set of M measures equal to:

$$\overline{U} = \frac{\sum_1^M g_i U_i}{\sum_1^M g_i}$$

In which g_i are weights that take different values depending on the model chosen to weigh the speed (g_i=1 no correction is introduced).

Several theoretical corrections and numerical simulations have been made on synthetic data, assuming tracers uniformly distributed in the fluid current, which indicate that it is right to use as weight the transit time (transit-time) of the particle in the measuring volume being inversely proportional to the velocity vector modulus regardless of the component that is actually measured. Transit time is easy to determine because it is the duration of the doppler signal of each individual particle and all modern processors are programmed to store this time along with the speed. The correction is valid regardless of the average sampling frequency (data-rate) and is as significant as the intensity of turbulent fluctuations.

11. USE OF THE INSTRUMENT

To describe the operation of the instrument, the laboratories of the Polytechnic of Bari (Prince... Innovative Processes for Energy Conversion) and in particular of a subsonic wind tunnel with square section and plexiglass test chamber also with 150mm square section. The air flow is driven through the duct by a fan driven by a variable frequency electric motor dictated by an inverter.

Figure 10.1 - Subsonic wind tunnel test from [10]

The Doppler laser anemometer used is the FlowLite-2D System from Dantec Dynamics, with a combination of blue ($\lambda_B = 488nm$) and green ($\lambda_G = 532nm$) beams. The two laser beams are generated by the FlowLite 2D unit and the signal is processed by the BSA-P60 processor. The laser head is moved through a 3-axis handling system driven by the Isel imc-S8 control unit.

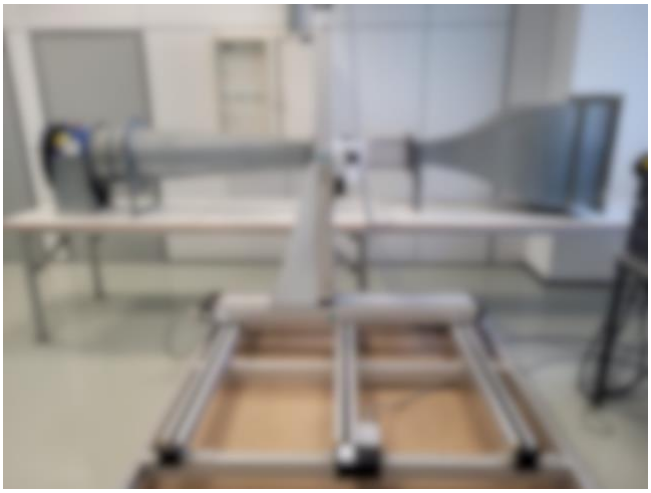

Figura 10.2a,b - Testing subsonic wind tunnel. a Sistema di movimentazione, b FlowLite 2D e Processore BSA-P60

Procedure for making the measurement:

1) Turn on the BSA P60 unit via the "Power" button, wait for the "ready" led to turn on and then connect via proprietary software;

2) Check that the shutter knob of the FlowLite 2D is on "Closed" then remove the laser head lens cover;

3) Turn on FlowLite 2D via Ignition Key by switching from "Off" to "On ON";

4) Turn on the control unit for handling the laser head (Isel imc-S8 unit);

5) Insert the USB stick into the PC to use the "BSA Flow Software" software license and launch it;

6) Click on "Browse for an existing project" and select the desired test file as shown:

Figure 10.3 - Screenshot of the BSA Flow Software

7) In the window "Device List" it is necessary to connect the units "Processor" and "Traversing system" through the command "Connect" previous interrogation with right click as shown in figure 10.4;

Figure 10.4 - Connection to the Processor and Traversing system from the BSA Flow Software

8) When connecting to traversing (laser handling system), pay attention to the fact that the last position assumed by the laser head is taken as the default axis source (x, y, z = 0). Therefore, a new origin must be identified at each ignition according to the specific case under consideration;

9) The position along the x-axis of the new origin can be identified with the help of a plate on which to visualize the convergence of the beams in the measuring volume and along z and y by moving the laser head, as shown below:

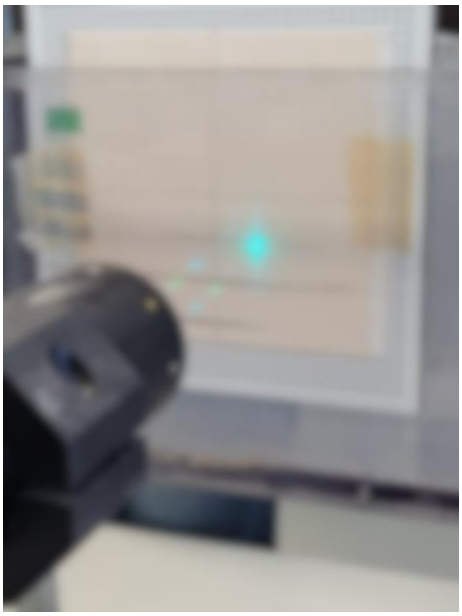

Figure 10.5 - Support system to evaluate the convergence of the beams.

10) To open the traversing controller you right-click on "traverse system-traverse controller", then the control window opens where, by clicking on "click here", the traversing can be moved by certain keys or by entering the coordinates;

(Traversing requires absolute coordinates, x_i are not entered but the x_i are directly compared to the 0 already assigned)

11) The traversing parameters can be displayed and modified as follows: in the "Device list" window click on "Traverse System". Or at the bottom left, in the window "Properties Traverse Driver" you can create a path to follow the laser head during the measurement procedure by listing a succession of positions that will be taken from the origin of the axes. These positions determine a measurement grid or dot matrix.

Figure 10.6 - Window of the BSA Flow Software for the insertion/modification of the parameters of Traversing.

12) To locate this matrix, place the shutter knob in the "Reduced" position. In this way it is possible to verify the positioning of the measuring volume given by the intersection of the beams without harming the operator's view;

13) Once the measuring grid is defined, the fan is switched on, which will generate a flow inside the duct. A smoke generator is activated upstream of the convergent inlet tract, which allows the addition of inseminating particles inside the flow;

14) In order to scan, you must move the shutter knob to the "open" position.

15) To conduct the scan, navigate to the "BSA F/P Application-Repetitive" shortcut bar.

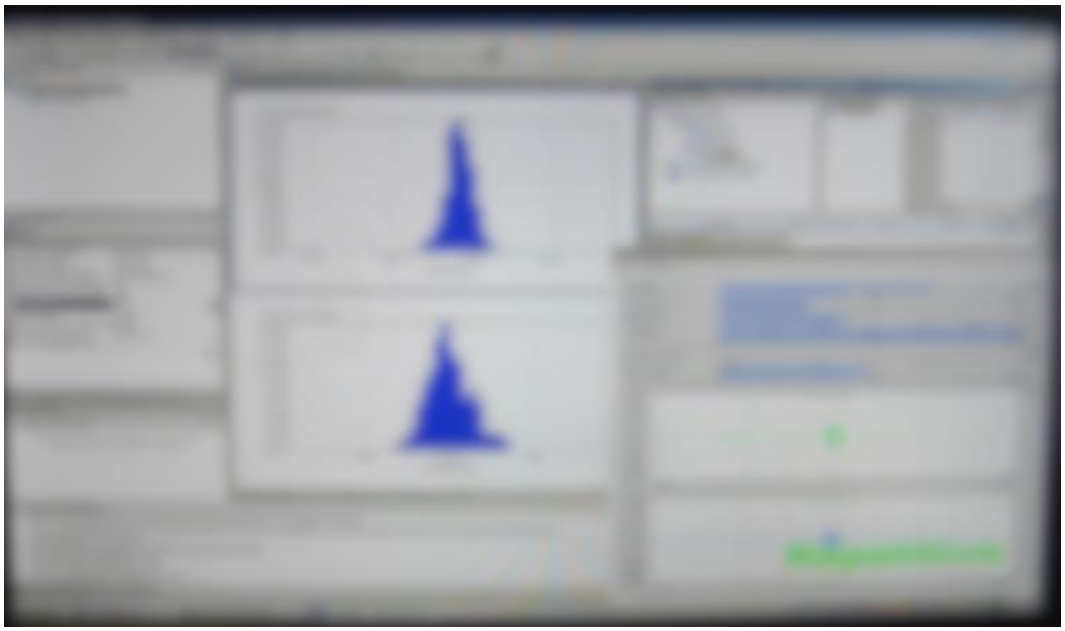

Figure 10.7 - Output of the measure on BSA Flow Software.

During the acquisition time window the software detects speed intervals, counts how many inseminating particles have a velocity that falls into those intervals and builds a histogram. In order for the measurement to be representative of the local flow velocity, the distribution of the samples must tend to a Gaussian; in fact, only in this case the measurements can be considered independent and repeatable;

16) Right-click on "Processor-System Monitor". A window appears in which you can view the "Data Rate" (usually around 1k) and the "Validation";

17) Outgoing software generates an Excel file as the following:

Version	DXEX v5									
Project	\Project1.da									
Date/Time	09:47:01									
Position	1	0,00 mm	-50,00 mm							
Region	Region1									
Row#	X [mm]	Z [mm]	Date_Time	Count {1}	Data Rate {1} [#/s]	Validation {1} [%]	LDA1-Mean [m/s]	LDA4-Mean [m/s]	LDA1-RMS [m/s]	LDA4-RMS [m/s]
1	-50	-50	09:47:01	2000	3909,086699	100	-2,790324774	-0,089680929	0,183068304	0,170843589
2	-31,8	-50,0	09:47:06	2000	2105,080215	99,04102325	-2,894965061	-8,13992E-06	0,188787067	0,200174821
3	0	-50	09:47:13	2000	540,277189	98,58065033	-2,874356157	-0,091885076	0,189998054	0,178075827
4	31,8	-50,0	09:47:22	572	57,37048489	99,32404327	-2,783812002	-0,244354094	0,222417301	0,206971813
5	50,0	-50,0	09:47:37	716	71,98159845	99,36916351	-2,621322256	-0,27115474	0,241833404	0,201393321
6	50,0	-31,8	09:47:51	379	38,05587687	96,92339325	-2,649900718	-0,343971156	0,222566884	0,196856284
7	31,8	-31,8	09:48:06	2000	260,1516588	98,84489441	-2,775072376	-0,130163864	0,213842415	0,216142875
8	0,0	-31,8	09:48:19	2000	882,2811961	98,98203278	-2,891772162	0,055565348	0,188650265	0,201562744
9	-31,8	-31,8	09:48:27	2000	2252,418918	100	-2,806908493	-0,059150102	0,201713141	0,195876682
10	-50,0	-31,8	09:48:32	2000	2743,843547	100	-2,807313547	-0,081909806	0,223493668	0,198107797
11	-50,0	0,0	09:48:39	2000	486,4942956	98,41410828	-2,754615694	-0,028859254	0,234810144	0,226186153
12	-31,8	0,0	09:48:47	2000	1634,706056	98,8555069	-2,851309033	0,114831037	0,193227186	0,188111403
13	0,0	0,0	09:48:54	2000	708,6825595	92,75171661	-2,814074217	0,046696074	0,213824439	0,237860855
14	31,8	0,0	09:49:02	502	50,85709427	98,91012573	-2,616223556	-0,167636097	0,283321125	0,272578634
15	50,0	0,0	09:49:17	393	39,61023667	97,73728943	-2,637091691	-0,651185074	0,261366781	0,237204941
16	50,0	31,8	09:49:33	398	40,26373863	98,45376587	-2,50702323	-0,60298629	0,244732217	0,255615392
17	31,8	31,8	09:49:48	1322	132,7245444	99,67033386	-2,410018975	-0,386748043	0,288561798	0,293635271
18	0,0	31,8	09:50:03	2000	504,5461356	98,98677063	-2,480950311	0,197117278	0,322173574	0,293519177
19	-31,8	31,8	09:50:13	2000	1273,375092	99,53874207	-2,662621309	0,090972737	0,270745204	0,186280155
20	-50,0	31,8	09:50:19	2000	2490,749026	100	-2,626563571	0,028523149	0,241894503	0,2356829
21	-50,0	50,0	09:50:24	2000	1859,546425	99,12332153	-2,538615585	-0,096783689	0,223150219	0,203941637
22	-31,8	50,0	09:50:30	2000	481,8482744	99,07157135	-2,530792222	0,100082065	0,239922145	0,18193022
23	0,0	50,0	09:50:40	1146	114,7227821	99,5933075	-2,491928871	0,03215746	0,282799332	0,216177042
24	31,8	50,0	09:50:56	28	2,844748146	100	-2,405635554	-0,253448005	0,26555306	0,27116765
25	50,0	50,0	09:51:12	0	2,844748146	100	-2,405635554	-0,253448005	0,252856189	0,27116765

Figure 10.8 - Excel measurement output.

In the output file you can read the positions of the grid points with their coordinates, the acquisition time, the number of tracer particles detected, the rate of particles that have passed through the measuring volume, a data validation index, the expected value of the speed components and the corresponding deviations.

12. ADVANTAGES, DISADVANTAGES AND APPLICATIONS

The LDA system has the following advantages and disadvantages:

- Does not require complex calibration procedures;
- Spacetime resolution comparable to that of the hot wire anemometer but provides point signal;
- System more robust than the anemometer;
- A better approach to the study of turbulence through random sampling;
- Non-intrusive even if in some cases the optical windows for the passage of laser beams can be more intrusive than the hole for a pitot;
- Need to choose appropriate tracer particles;
- Cost not indifferent.

Below will be some applications taken from scientific articles to confirm the utility and versatility of the LDA instrument. The articles will refer to two separate applications, namely: improvement of integrated navigation systems and study of wind speed in areas difficult to access.

a) Ground speed of a vehicle

In recent years, the Doppler laser anemometer using the single beam configuration has been used for measuring the ground speed of vehicles. In particular, the transfer function of this configuration is as follows::

$$V = \frac{f_D \lambda}{2 \cos \theta}$$

Essentially, the vehicle's speed relative to the ground is determined by the Doppler frequency, the beam angle and the laser wavelength. The speed is then correlated and affected by the pitch or angle of attack to the ground of the vehicle. To eliminate this the influence on the speed measurement has been developed a two-beam LDA technology called Pitch-Independent LDA whose scheme is shown in figure 12.1.

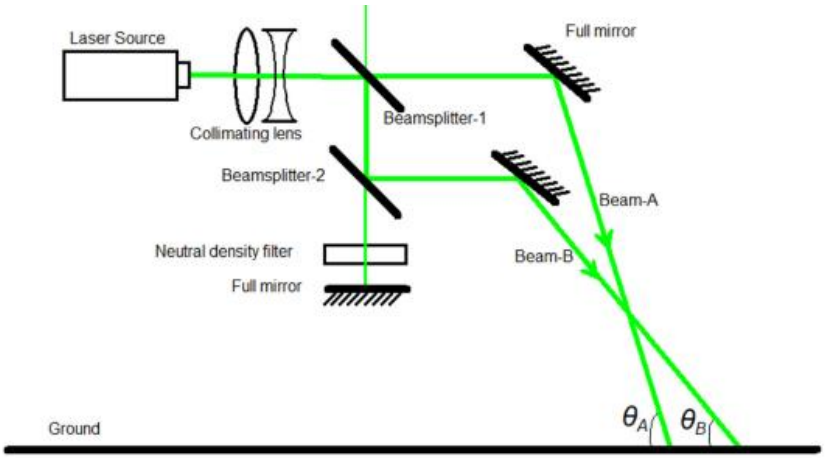

Figure 12.1 - Pitch-Independent LDA configuration from [7]

The light source is a green laser (TEM_{00}) with a wavelength of 532 nm. The laser beam is divided by the beamsplitter-1 into two beams transmitted to the ground through two mirrors and determining different ground angles.

The transfer function of the new configuration will be:

$$\begin{cases} V = \dfrac{\lambda f_{DB}}{2}\sqrt{1+\left(\dfrac{1}{\tan(\Delta\theta)}-\dfrac{1}{\sin(\Delta\theta)}\dfrac{f_{DA}}{f_{DB}}\right)^2} \\ \\ \Delta\theta = \theta_A - \theta_B \end{cases}$$

As you can see from the last report, the pitch-independent LDA depends on the two Doppler frequencies and the difference between the two angles on the ground, which remains constant at the assigned configuration. Otherwise, in the single reference-beam configuration the angle of attack of the vehicle to the ground can change and this affects the speed measurement.

The test used to test this new configuration consists in subjecting three LDA systems, two of which have single reference-beam and one with pitch-configurationindependent to the speed measurement of a treadmill that is driven at a constant speed of 6m/s. The ground angle of attack shall be changed during the test to assess any deviations in the speed readings. The result of this test is shown below:

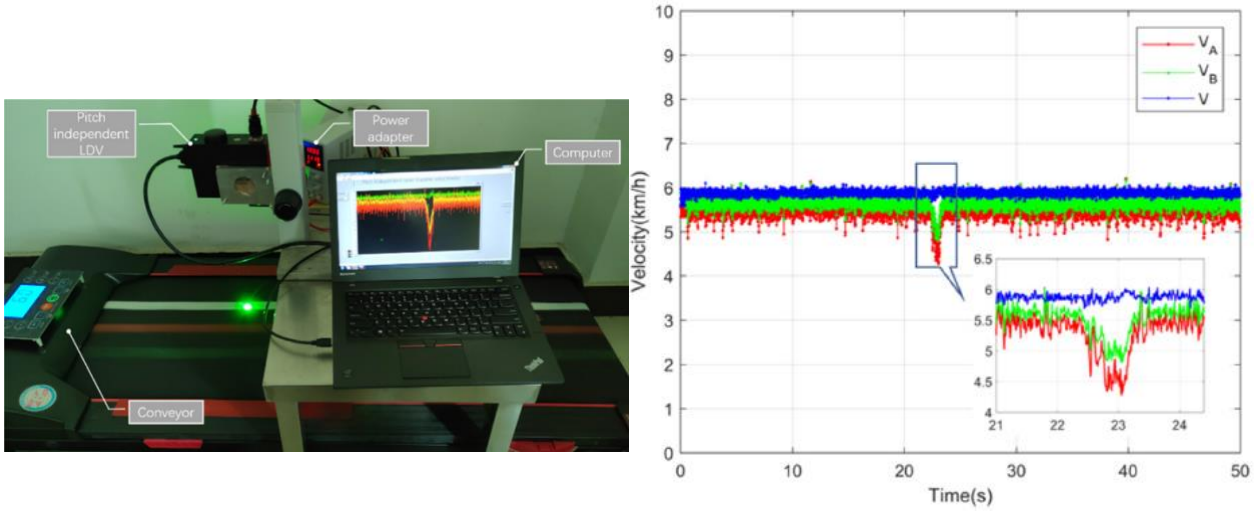

Figure 12.2 - Results of the tests carried out. A,B single beam and blue Pitch-Independent configuration from [7].

Theoretical analysis and experimental tests show improved speed estimation compared to traditional LDA systems and possible implementation of configuration in navigation and location systems.

b) Miniature LDA for wind speed measurement and dust concentration on Mars

Suspended dust is a dominant component of the Martian environment; it affects atmospheric circulation and, due to its highly oxidizing nature, is dangerous to space exploration equipment. To study the behaviour of such dust in a Martian environment, the quantification of wind speed and dust charge is fundamental.

The existing data on in situ measurements of Martian dust were largely acquired first by the two Viking Landers (1976 and 1982 respectively) and then by the Pathfinder lander (1997). The only proven method for measuring wind speed on such Landers is hot-wire anemometry.

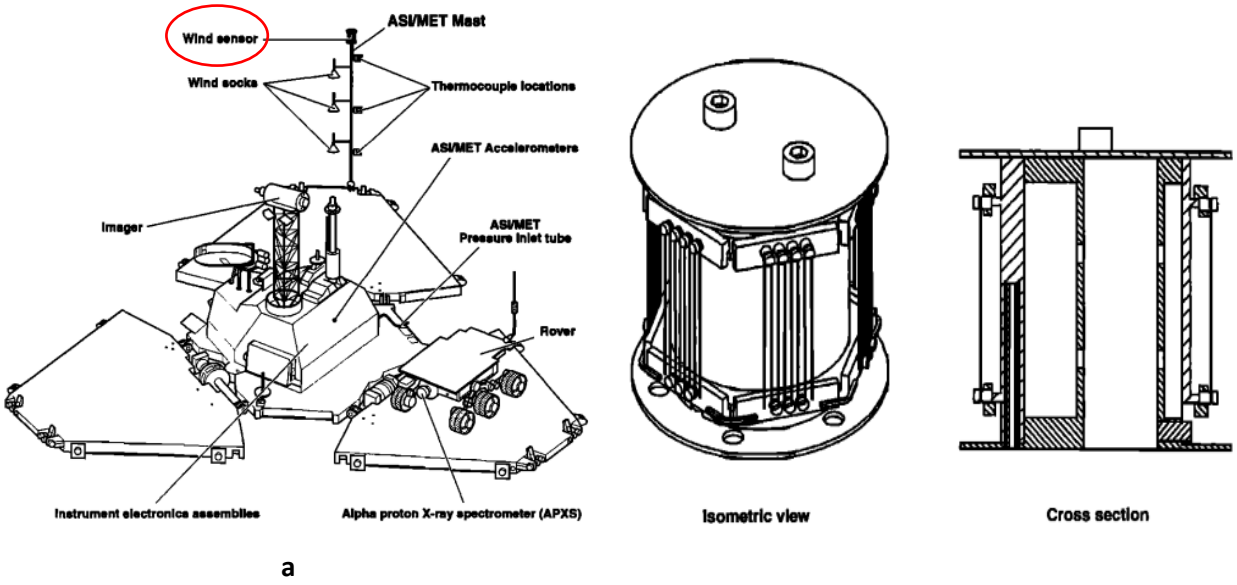

Figure 12.3a,b - Pathfinder lander. a Overall drawing b Wind sensor in detail from [9]

As you can see from figure 12.3b, in the Pathfinder lander (1997), the wind sensor consists of six identical wire anemometers (Hot-wire anemometer with elements of 0.9 Pt/0.1 Ir alloy, 65-µm-diameter wire arrayed around a circular cylinder 2.7 cm in diameter). When exposed to wind, the overall cooling of the sensor cables depends on wind speed, while the cooling differences between individual wires depend on wind direction.

However, the hot wire anemometer requires direct contact with the gas and is susceptible to contamination (e.g. dust). Its operation also depends on the temperature, pressure and composition of the gas. In case of low wind conditions it works badly given the poor capacity of the fluid, in this condition, to cool the sensor.

In recent times, Laser Doppler Anemometers have been widely used for wind measurement in the Earth field, and therefore their application in the Martian field has been started as indicated in [8].

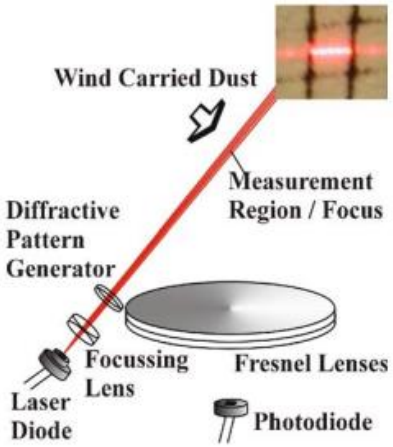

Figure 12.4 - laser miniature anemometer scheme from [8]

The possible use of an LDA system, of which the diagram is shown in figure 12.4, would have a double advantage compared to the hot wire anemometer in the application in the Martian field, or:

- Non-contact speed (V) measurements with the advantage of not exposing the measuring sensor to the Martian oxidizing atmosphere;

- The possibility of obtaining information about the particle concentration (k_d) of Martian dust by the same measurement of wind speed. In fact, by simply counting the number of particles sampled in the unit of time (C) and taking into account the area (s) crossed by the latter, which is defined only by the optical configuration, the concentration can be estimated as follows::

$$k_d = \frac{C}{sV}$$

13. BIBLIOGRAPHY

- [1] H.-E. Albrecht, Borys, N. Damaschke, C. Tropea – Laser Doppler and Phase Doppler Measurement Techniques;
- [2] G. P. Romano – Appunti di Aerodinamica Sperimentale
- [3] E. Doebelin – Metodi e Strumenti di Misura;
- [4] M. Napolitano, P. De Palma, G. Pascazio – Appunti di Gasdinamica
- [5] L'effetto Doppler – Articoli – castfvg.it
- [6] Dantec Dynamics https://www.dantecdynamics.com
- [7] Pitch independent vehicle-based laser Doppler velocimeter by Xiaoming Nie, Jian Zhou
- [8] A miniature laser anemometer for measurement of wind speed and dust suspension on Mars by J.P. Merrison, H.P. Gunnlaugsson, J. Jensen, K. Kinch, P. Nørnberg, K.R. Rasmussen
- [9] The atmosphere structure and meteorology instrument on the Mars Pathfinder lander Alvin Seiff, James E. Tillman, James R. Murphy, John T. Schofield, David Crisp, Jeffrey R. Barnes, Clayton LaBaw, Colin Mahoney, John D. Mihalov, Gregory R. Wilson, and Robert Haberle
- [10] Validation of a method for fluid flow rate measurement in square ducts by means of laser velocimetry L. Fabbiano, G. Dinardo, G. Vacca